Russian Geology and Geophysics © 2020, V.S. Sobolev IGM, Siberian Branch of the RAS
Vol. 61, No. 4, pp. 428–443, 2020 *DOI:10.15372/RGG2019107* *Geologiya i Geofizika*

Negative $\delta^{13}C$ Excursions in Foraminiferal Records: The Holocene History of Methane Events in the Central Sea of Okhotsk

S.P. Pletnev[a], Yonghua Wu[b], A.V. Romanova[c], V.K. Annin[a], I.V. Utkin[a, ✉], O.F. Vereshchagina[a]

[a] *V.I. Il'yichev Pacific Oceanological Institute, Far Eastern Branch of the Russian Academy of Sciences, ul. Baltiiskaya 43, Vladivostok, 690041, Russia*

[b] *First Institute of Oceanography, Jindao, 266061, China*

[c] *Far East Geological Institute, Far Eastern Branch of the Russian Academy of Sciences, pr. 100-letiya 159, Vladivostok, 690022, Russia*

Received 13 July 2018; received in revised form 12 March 2019; accepted 21 March 2019

Abstract—Several negative $\delta^{13}C$ excursions in benthic foraminifera from gas-bearing core LV50-05 sampled offshore on the eastern slope of Sakhalin Island, Sea of Okhotsk, in an area of active methane seepage record the local history of methane events (ME). The core chronostratigraphy has been contrained from AMS ^{14}C ages and biostratigraphic data. Benthic foraminifera (*Nonionellina labradorica* and *Uvigerina parvocostata*) from some core intervals show normal marine $\delta^{13}C$ values about –1‰ but some intervals are marked by extremely depleted compositions as low as –34.5‰ $\delta^{13}C$ (relative to VPDB). The negative $\delta^{13}C$ excursions are interpreted as a record of seabed methane emanation during primary and secondary biomineralization of carbonate foraminifera. The results reveal four Holocene methane events (ME) in the area: two brief (ME-1 at 700–900 yr BP and ME-2 at 1200–1400 yr BP) and two long (ME-3 at 2500–4700 yr BP and ME-4 at 7400–10000 yr BP) events.

Keywords: benthic and planktonic foraminifera, oxygen and carbon isotope compositions, methane, methane emission, Sea of Okhotsk

INTRODUCTION

The discovery of extremely abundant gas hydrates in permafrost and epicontinental seas calls for understanding the role of crystalline gas forms in the past, present, and future Earth's history. Gas hydrates store enormous resources of methane (up to 98%) and can become an alternative source of fuel hydrcarbons. Perturbation to the primary burial conditions may lead to dissociation of gas hydrates and release of free methane, second major greenhouse gas blamed for global warming. Increased methane emanation has been invoked as a cause of mass extinctions in the Cretaceous, Paleocene/Eocence boundary, Pleistocene, and Holocene periods (Dickens et al., 1995; Hill et al., 2004; Panier et al., 2014).

Methane seepage through seabed produces particular ecosystems in which bottom and pore waters, as well as living organisms, are depleted in the heavy isotope ^{13}C (Hill et al., 2004; Levin, 2005). Therefore, the ratio of ^{13}C and ^{12}C isotopes ($\delta^{13}C$) in fossil calcareous organisms at sites of prolonged methane seepage may store a record of methane fluxes. Benthic foraminifera are a good methane tracer (Sen Gupta et al., 1997). These unicellular organisms with calcic exoskeletons live at different depths in oceans, have a long history, and are abundant in sediments. Having studied the carbon isotope composition of fossil foraminifera, Kennett et al. (2000) hypothesized that the latest Holocene warming began with a considerable increase of atmospheric methane. Yet, neither the available data from geological sections at the sites of methane seepage nor the knowledge of its history are sufficient to prove or disprove this hypothesis.

The stable isotope compositions of extant foraminifera show correlation between methane seepage and $\delta^{13}C$ in some species (Kennett et al., 2000; Rathburn et al., 2000, 2003). The $\delta^{13}C$ difference in the same species living currently inside and outside seepage areas is minor (from –0.3 to –1.0‰ (Pletnev et al., 2014) in the Sea of Okhotsk) though poorly constrained (Rathburn et al., 2000, 2003; Bernhard et al., 2010), but it may reach –40‰ in fossil foraminifera (Torres et al., 2003; Uchida et al., 2008). Possible controls of the foraminiferal isotope record remain controversial. According to some models, living foraminifera build their calcite exoskeletons by extracting carbon from low-$\delta^{13}C$ pore water (Sen Gupta et al., 1997; Panieri et al., 2014). Other models attribute the $\delta^{13}C$ depletion to consumption by methanotrophic bacteria which are a food source for foraminifera (Torres et al., 2003; Hill et al., 2004). As shown lately, methane-derived diagenetic authigenic carbonate (MDAC) with low $\delta^{13}C$ values can precipitate over dead

✉ Corresponding author.
E-mail address: utkin@poi.dvo.ru (I.V. Utkin)

foraminifera and mask the $\delta^{13}C$ signal from alive foraminifera (Torres et al., 2003; Panieri et al., 2016). The records of $\delta^{13}C$ and methane emission have been studied for the cases of alive and fossil foraminifera in different areas of the World Ocean. The Sea of Okhotsk, where large gas hydrate resources were predicted (Soloviev et al., 1994) after the discovery of methane seepage (Zonenshain et al., 1987), is an advantageous area for this research. Gas hydrates are especially abundant offshore along the northeastern continental slope of Sakhalin Island, where international geological and geophysical surveys discovered numerous methane seeps in bottom waters and shallow sediments (Hachikubo et al., 2011; Kim et al., 2013; Minami et al., 2013; Akulichev et al., 2014). Some publications on the Sea of Okhotsk concern the effect of methane on the isotope systematics of alive foraminifera (Ishimura et al., 2012; Pletnev et al., 2014), chemistry of foraminifera tests (Husid et al., 2013), and negative $\delta^{13}C$ excursions in bottom sediment core record (Lembke-Jene et al., 2007, 2017; Wu et al., 2014).

We report data collected during the 50th cruise of R/V Akademik Lavrentyev in 2010, which were used to estimate Holocene methane fluxes from benthic foraminiferal $\delta^{13}C$ patterns in core LV50-05 (Fig. 1), which was analyzed comprehensively by several methods. We also discuss methodological issues related to carbon isotope analysis in some species of benthic foraminifera at methane seepage sites in the Sea of Okhotsk.

OCEANOGRAPHY AND GEOLOGY OF THE STUDY AREA

The Sea of Okhotsk currently has low water temperatures, hard ice conditions, and high primary productivity. Its surface hydrography is controlled by large cyclonic turnover (Fig. 1). Warm Pacific waters penetrate into the Sea mainly through the Krusenstern Strait (1900 m sea depth) and with the Kamchatka current which flows along the West Kamchatka shore and then mixes with cold waters of the northwestern shelf. The East Sakhalin current flows around northern and eastern Sakhalin and turns toward the Kuriles in the south.

In the cold season, low temperatures and salt separation from sea ice lead to the formation of dense shelf waters in the northwestern Sea of Okhotsk (Itoh et al., 2003) which maintain renewal of intermediate waters and oxygenate deep waters (Tsunogai et al., 1995).

The site LV50 (Fig. 1) is exposed to the effect of the East Sakhalin current and freshwater of the Amur River which carries about 14 km^3 of sediment load annually, or two or three times the total discharge of all Siberian rivers (Anikiev et al., 2001). The Amur input causes stable water stratification with the formation of a dichothermal layer at a depth of 50 to 150 m in the summer (Freeland et al., 1998). Seasonal ice at the site forms since November and holds about 200 days in a year.

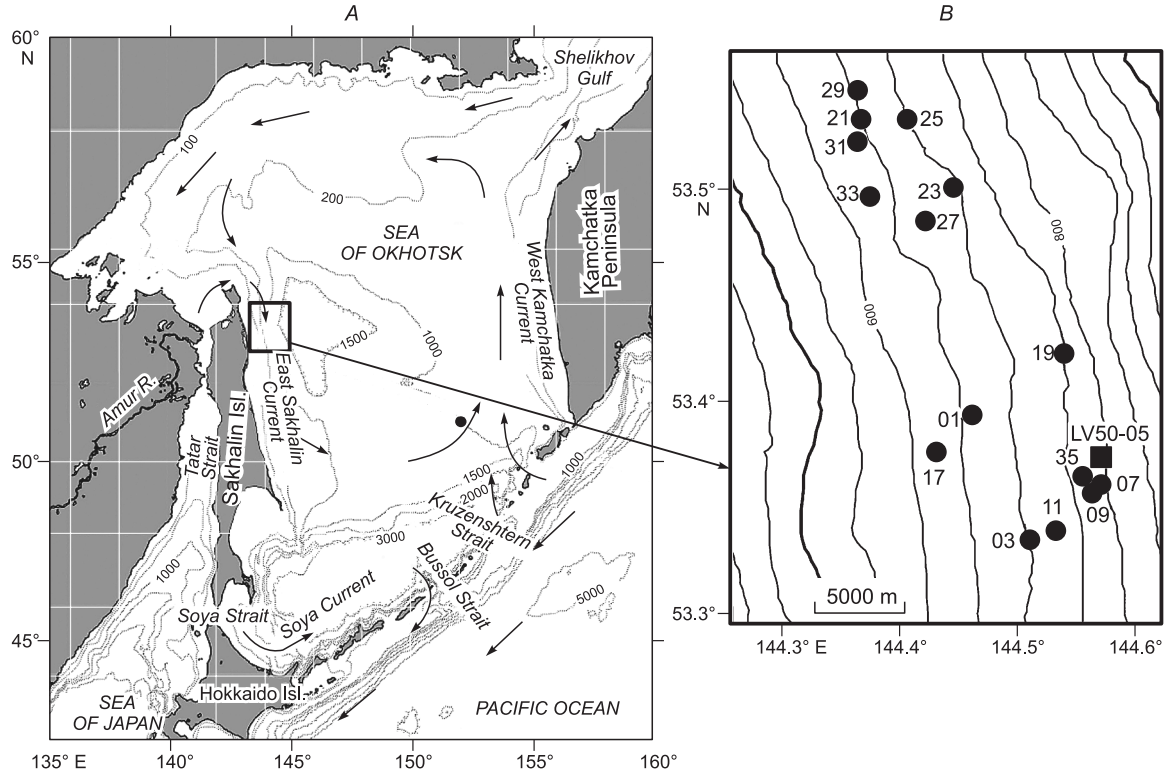

Fig. 1. *A*, Bathymetric map of the Sea of Okhotsk, with main straits and surface currents; *B*, sampling sites of LV50-05 and other cores mentioned in the text.

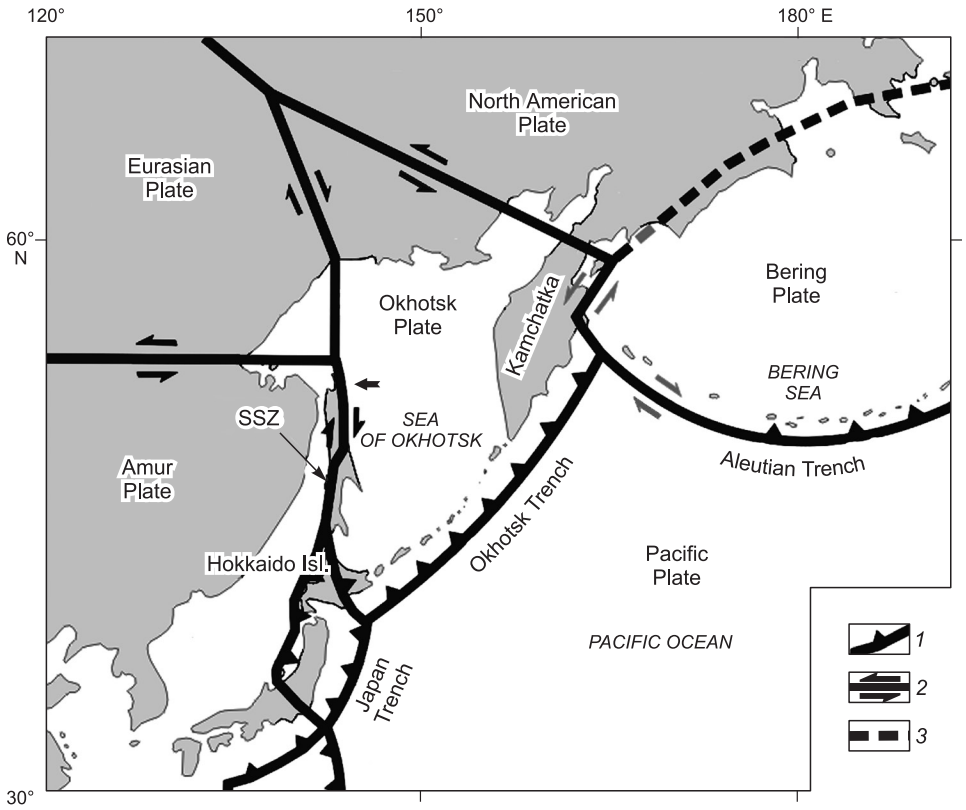

Fig. 2. Recent plate boundaries of the northwestern Pacific, after (Wong et al., 2003). *1*, direction of subduction; *2*, plate motion; *3*, plate boundaries; SSZ, Sakhalin shear zone.

High local primary productivity (mainly diatoms) is due to good illumination and high inputs of nutrients and iron with the Amur (Sorokin and Sorokin, 1999). Much carbon is transported by the Amur River and intermediate waters (Kitani, 1973). Low bottom water temperatures, high deposition rates, and large organic inputs favor the formation of methane in the shallow sediments of the region (Soloviev et al., 1994).

The Sea of Okhotsk basin is mainly located within the Okhotsk plate that borders the Eurasian, North American, Amur, and Pacific plates along transform faults (Fig. 2). The continental slope of Sakhalin is composed of 9–14 km thick Eocene–Holocene faulted sediments (Kharakhinov, 2010).

These sediments which have undergone compression and heavy deformation provide storage and migration of gas. Methane seeps (gas flares) trace numerous mud volcanoes, pockmarks, gas hydrates, etc. (Kim et al., 2013; Akulichev et al., 2014). The Holocene deposition environment was similar to the present conditions (Wong et al., 2003). High deposition rates (0.5–1.0 m per 1 kyr) indicate the leading role of clastic transport in the area (Biebow et al., 2003).

MATERIAL AND METHODS

The 495 cm long core LV50-05 was retrieved offshore on the northeastern continental slope of Sakhalin from a sea depth of 785 m during the LV50 cruise of R/V Akademik Lavrentyev in June 2010. The samples of bottom sediments (about 30–50 g) were collected at every 10 cm, wet sieved to >0.063 mm, and the residues were dried at 40 °C.

Planktonic and benthic foraminifera (PF and BF, respectively) were analyzed under an *MBS-10* binocular. Samples with counts exceeding 300 individuals were quartered. The biostratigraphic analysis of the core was based on foraminifera numbers counted as individuals per 1 g of dry sediment and on numbers and relative percentage of species in each of 49 samples. Changes in the foraminiferal taphocenoses were estimated using the PAST software (Harper, 1999) according to three standard indices: Shannon diversity, Fisher's alpha, and equitability.

AMS ^{14}C dating was applied to foraminifera tests (*Uvigerina peregrina parvocostata,* hereafter *U. parvocostata*) and fragments of bivalve shells. Whole well preserved tests and shells free from MDAC overgrowths were selected for analysis in order to reduce chronological inconsistency caused by authigenic carbonate precipitation. All samples (>10 mg of foraminifera and >100 mg of mollusks) were measured for δ^{13}C. Both foraminifera and mollusks were dated in the 300–305 cm interval for comparison. The isotope measurements were performed in the Woods Hole Oceanographic Institution (USA). All AMS ^{14}C ages were calibrated to calendar years (Fairbanks et al., 2005) with regard to a regional reservoir effect of 950 years (Keigwin, 1998).

Oxygen and carbon isotope compositions were studied in three benthic foraminifera species (*U. parvocostata, Valvulineria (V.) sadonica* and *Nonionellina (N.) labradorica*), which are tolerant to the conditions of methane seepage in the Sea of Okhotsk (Pletnev et al., 2014). We selected 2-4, 2-6 and 2-8 tests of *U. parvocostata, V. sadonica and N. labradorica*, of 1, 0.4–0.8 mm and 0.4–0.6 mm in size respectively. The tests were treated with ≥ 99.7% ethanol in a Branson-200 ultrasonic bath. The stable isotope measurements were run on a *Finnigan-Mat 253* mass spectrometer at the Laboratory of Marine Geology of Tongji University (Shanghai), to an accuracy of 0.05‰ for $\delta^{13}C$ and 0.07‰ for $\delta^{18}O$. All values are quoted in per mill on the international Vienna Pee Dee Belemnite (VPDB) scale defined by the NBS-19 reference material (Cheng et al., 2005).

Ultrastructural changes in foraminifera which trace the patterns of secondary calcite precipitation and dissolution were analyzed on a Carl Zeiss *EVO 50 XVP* scanning electron microscope at the Laboratory of Geochemistry of the Far East Geological Institute (Vladivostok).

Methane in the core samples was measured by the head space equilibration technique following the standard procedure (Jin et al., 2011). The gas content was determined on a *Crystal-Lux 4000M* gas chromatograph (Russia), to accuracy within 10%.

RESULTS

Lithology and age model. The core LV50-05 (Jin et al., 2011) mainly consists of olive green diatom mud and clastic sediments and comprises three units: (1) 0–120 cm: clayey diatomaceous ooze; (2) 120–290 cm: homogeneous silty-clay mud and diatoms; (3) 290–495 cm: dense silty-clay mud containing bivalve shells and soft (310–375 cm) or hard (430–455 cm) carbonate precipitates (Fig. 3). The soft varieties are 0.5–2.5 cm round concretions of consolidated carbonate sediments, which may represent an early stage of hard concretions. The percentage of diatom mud increases markedly above 270 cm. The sediments at 0 to 360 cm core depths are massive, without signatures of slumping, but have a vesicular structure (Fig. 4) below 360 cm due to methane hydrate dissociation.

Past methane emanation events are commonly dated by the radiocarbon age method. Dating of calcareous fossils at

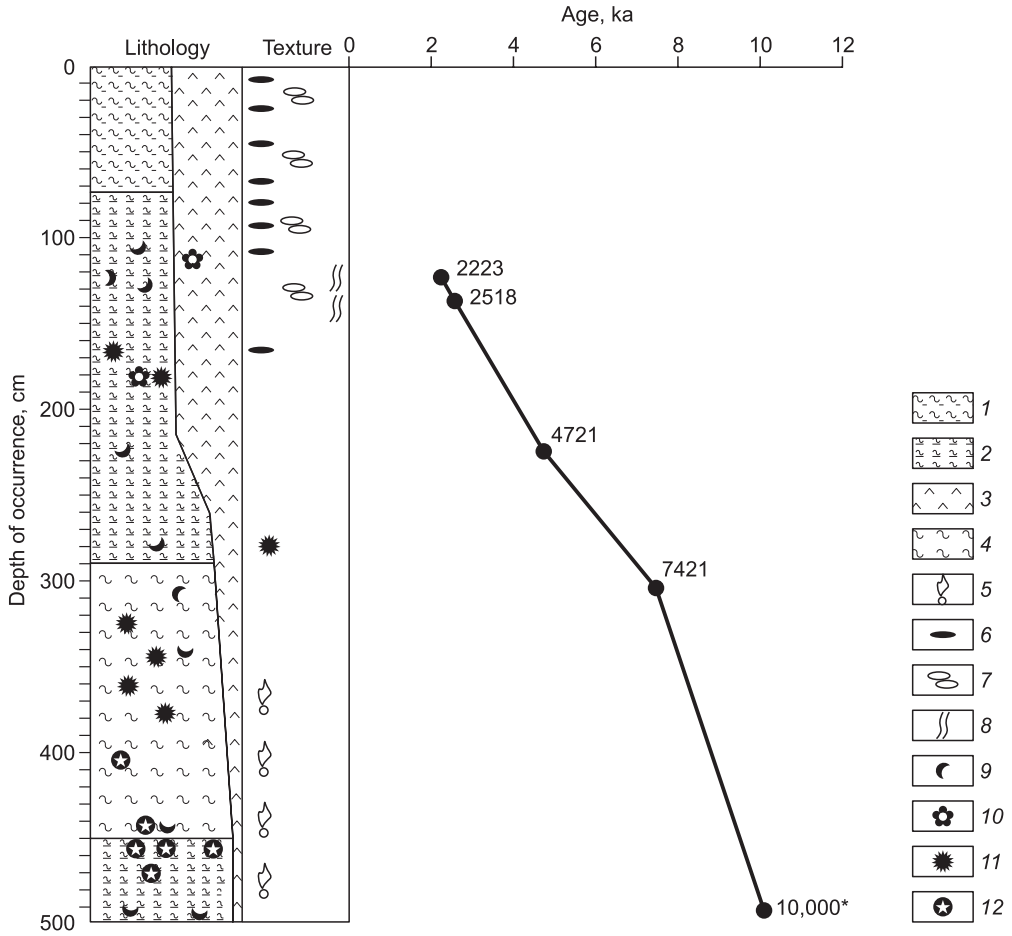

Fig. 3. Lithology and age model of core LV50-05. *1*, clayey silt; *2*, silty clay; *3*, diatomaceous ooze; *4*, clay; *5*, gas-saturated sediments; *6*, hydrotroilite layers and lenses; *7*, bedded-spotted sediments; *8*, bioturbation; *9*, shell fragments; *10*, coccolites; *11*, soft carbonate precipitates; *12*, hard carbonate precipitates.

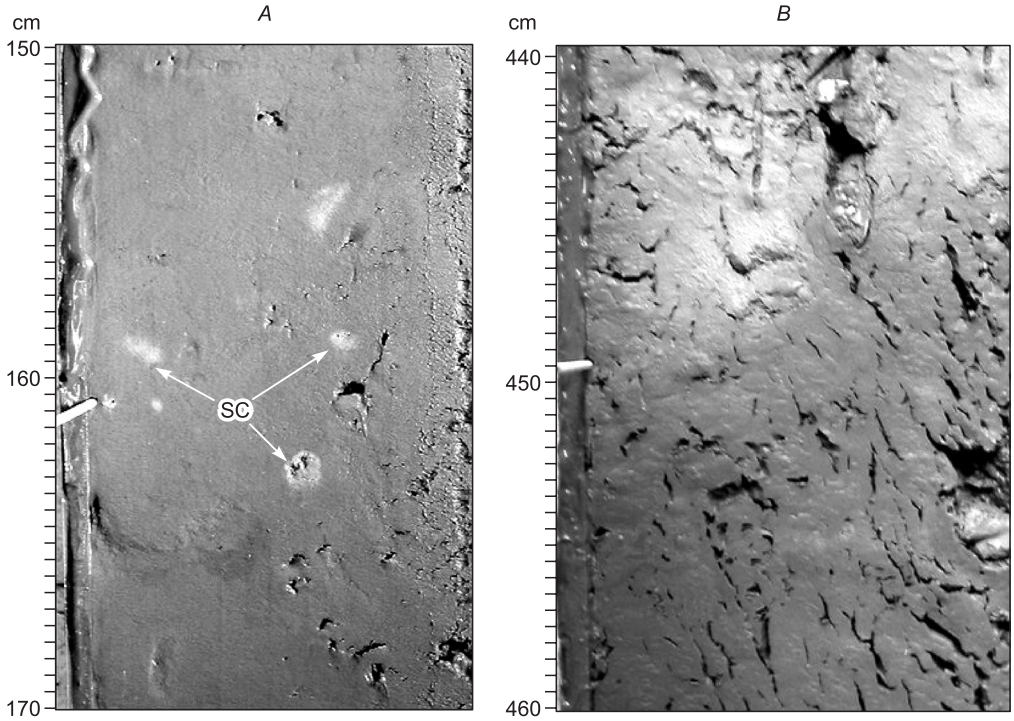

Fig. 4. Textures of cored sediments. *A*, Massive texture and traces of soft carbonate precipitates (SC); *B*, vesicular (gas-saturated) texture.

methane seepage sites has its specificity: the ^{14}C content of the foraminiferal carbonate should reflect that of seawater DIC when the foraminifera were alive (Uchida et al., 2008).

The carbon isotope composition is around $\delta^{13}C = 0 \pm 3‰$ in common marine carbonates (Hoefs, 1980; Arslanov, 1987) and <–3.0‰ in methane-derived varieties. Living organisms may build their carbonate exoskeletons using fossil carbon from deep thermogenic methane which has been ^{14}C-free since long ago. This leads to underestimation of total ^{14}C in live foraminifera and overestimation of their calculated age (Aharon et al., 1997; Logvina et al., 2012): the greater the methane-derived carbonate component the larger the age error. The foraminifera ^{14}C ages may be also biased by a component of methanotrophic bacteria they consume in variable amounts or by the presence of MDAC in fossil shells. Depleted $\delta^{13}C$ (<–3‰) in carbonates indicate that the ages require correction.

Six out of eight obtained AMS ^{14}C dates show linear depthward increase and two dates (OS-117586 and OS-117590) are inverse (Table 1). The core is free from signatures of slumping or bioturbation, which rules out mixing of fossils of different ages. The age inconsistency may be due to different objects of dating: foraminifera and mollusks. Benthic foraminifera are more suitable for AMS dating than mollusks (Heier-Nielsen et al., 1995), and species of the *Uvigerina* genus are less prone to MDAC than mollusks (Logvina et al., 2012) and than *N. labradorica* (Cook et al., 2011). Our results support these inferences: $\delta^{13}C$ is < –3‰ in almost all mollusk shells but is about the normal marine values in foraminifera. For this reason, we have excluded four dates with $\delta^{13}C$ < –3‰ from the analysis and considered valid the AMS ^{14}C ages from the core depths 122, 130–135, and 220–225 cm. The age of the 300–305 cm interval appears to be slightly biased: overestimated lower age bound of 11436 ± 93 years BP for OS-117526, in which MDAC may be responsible for depleted $\delta^{13}C$ (Table 1). The age of the core base is rather around 10 kyr, as confirmed by our biostratigraphic analysis (see below), and the mean deposition rate is about 50 cm per 1000 years (Fig. 3).

Methane in bottom sediments. Methane in bottom sediment cores is characterized with reference to the sulfate-methane interface (SMI) that separates layers with background and high methane concentrations and marks the zone of anaerobic methane oxidation (AOM) where sediments are oxidized by CH_4 methanotrophic bacteria and methane-derived carbonate concretions can form (Borowski, 1999; Ussler and Paull, 2008). The LV50-05 sample has the SMI zone at the 300 cm core depth (Fig. 5).

The SMI profiles from the LV50 site are of four groups (Fig. 6). *Group a*: shallow cores containing gas hydrates, with SMI at 25–60 cm which formed early during gas hydrate dissociation and anaerobic oxidation of methane. *Group b*: gas-bearing sediments, with variable SMI depths corresponding to sampling depths at a flank of a methane-hydrate structure. *Group c1* (solid line on the left): background methane contents (0.01–1 ml/L) which are insufficient for modern gas hydrate formation or represent the stage after complete cessation of hydrate dissociation and

Table 1. AMS ^{14}C and calibrated calendar ages in core LV50-05

Sample ID	Core depth, cm	Material	Uncorrected AMS $\delta^{14}C$ age, m	$\delta^{13}C$, ‰	Calibrated calendar age, yr	Calibration version
OS-117588	122	Mollusk	3150 ± 20	–1.13	2223 ± 54	Fairbanks0107
OS-117586	130–135	Foraminifera	3400 ± 25	–1.49	2518 ± 102	Fairbanks0107
OS-117585	160–165	Mollusk	3150 ± 20	–3.06	*2223 ± 54*	Fairbanks0107
OS-117591	220–225	Foraminifera	5110 ± 20	–2.03	4721 ± 62	Fairbanks0107
OS-117589	280–285	Mollusk	7710 ± 25	–6.23	*7607 ± 21*	Fairbanks0107
OS-117590	300–305	Mollusk	8190 ± 30	–4.95	*8040 ± 41*	Fairbanks0107
OS-117790	300–305	Foraminifera	7450 ± 30	–3.49	7421 ± 20	Fairbanks0107
OS-117526	490–495	Mollusk	10950 ± 30	–6.81	*11436 ± 93*	Fairbanks0107

Note. Biased AMS ^{14}C ages are italicized.

AOM. *Group c2* (dash line on the right): sediments from a site of methane emanation into water (1 to 120 ml/L); both varieties of group *c* lack SMI.

Foraminifera. The core was sampled in the zone of oxygen minimum influenced by the East Sakhalin current. These facts cause specificity of the distinguished benthic foraminifera assemblages which is especially common to oxygen-depleted high-productive continental slopes of the Sea of Okhotsk (Saidova, 1997).

The foraminifera numbers vary over the core depth (Fig. 7): they are absent or sporadic in the intervals 310–390, 440–445, 460–465, and 480–485 cm. The BF and PF abundance peaks coincide within the 305–300, 275–270, 225–210, 185–180 and 135–130 cm intervals. The BF peak of 63 specimens per 1 g of dry sediment falls within 220–225 cm and that of PF (>100 individuals) is within 180–185 and 130–135 cm core depths. Foraminifera have well preserved tests with distinct morphological signatures only between 0 and 135 cm, but the numbers of yellow and brown foraminifera with traces of corrosion increase toward the core bottom.

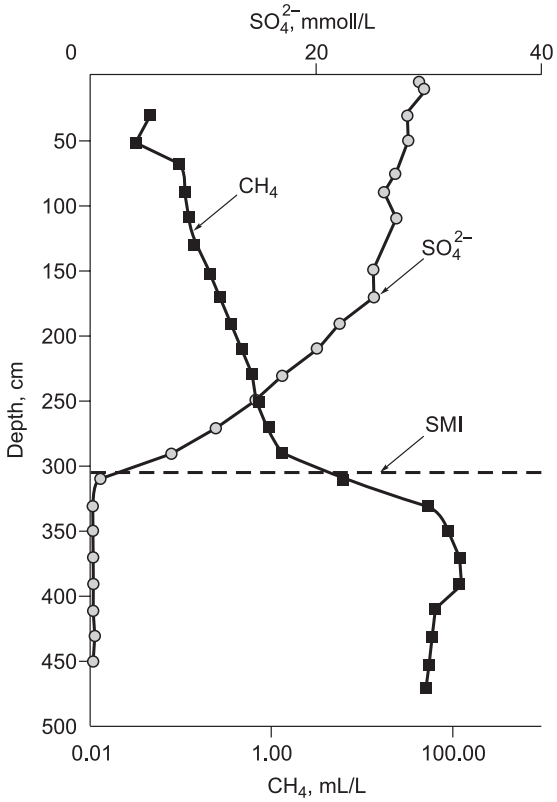

Fig. 5. CH4 and SO_4^{2-} profiles and SMI position in core LV50. SO_4^{2-} is according to (Minami et al., 2013).

We identified 46 benthic and 6 planktonic species of foraminifera. The species *U. parvocostata* Saidova, *Cribroelphidium batiale* (Saidova), *Cibicidoides borealis* Saidova, *N. labradorica* (Dawson), *V. sadonica Asano,* and *Pullenia sphairoides* (Dawson) predominate among benthic taxa, while Subarctic *Neoglobogudrina pachyderma sin*, Ehrenberg (70–90%), and Boreal *Globigerina bulloides* Orb. (10–25%) totally exceed 90% among planktonic species. The foraminifera taphocenoses in the core are very similar to the extant fauna at the LV50 site (Saidova, 1997; Pletnev et al., 2014), which prompts that the sediments are no older than the Holocene.

The core comprises three foraminifera units: 495–300, 300–135 and 135–0 cm. The foraminifera numbers (counted as number of tests per 1 g of dry sediment) are the lowest in the 495–300 cm interval: 3–12 and 1–6 for PF and BF, respectively. Benthic foraminifera belong to six *in situ* species (*U. peregrina, Retroelphidium subclavatum, N. labradorica, Cr. batiale, Epistominella pacifica, V.sadonica*) and two species (*Cr. asterineum, Buccella granulata* et al.) brought by ice rafting or gravity sliding of sediments. The planktonic species are mostly Subarctic *N. pachyderma sin*. (>87%). The low foraminifera numbers in this interval may result from poor inputs of nutrients and warm surface waters from the Sea of Japan and the Pacific. Judging by the lack of dramatic abundance changes at 14 and 11 kyr BP known for the Sea of Okhotsk (Seki et al., 2004), the interval was deposited after the Pleistocene termination events, most likely during the Preboreal and Boreal phases of the Early Holocene.

Interval 300–135 cm. Foraminifera increase both in the number of species (to 28) and in abundance (numbers of 63 and 121 for BF and PF, respectively). The assemblages almost all over the core include high percentages of foramin-

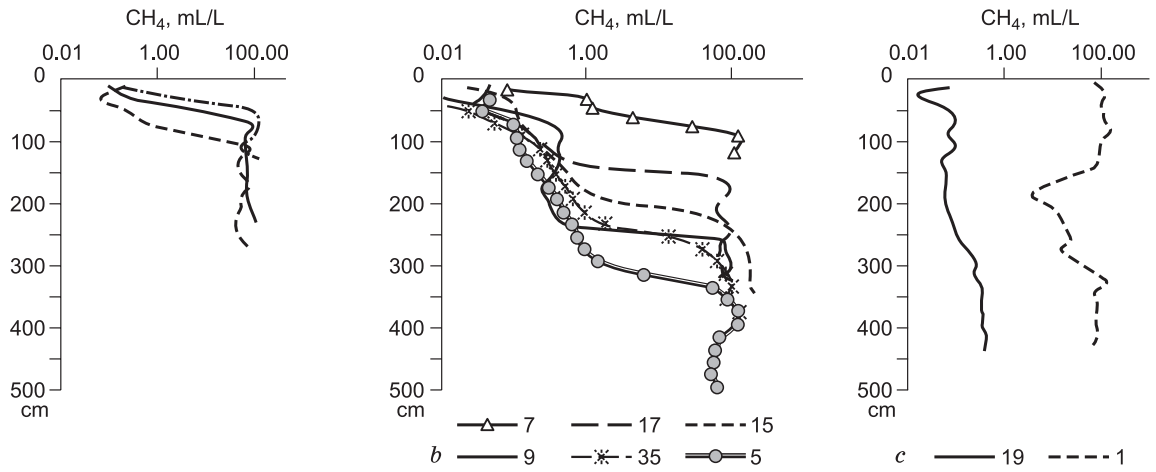

Fig. 6. Methane profiles in cores from site LV50. Profiles are grouped as described in text, groups *a*, *b*, *c* (Fig. 1).

ifera species that record high organic inputs to bottom waters and oxygen depletion: *U. parvocostata, N. labradorica,* and *Brizalina pacifica*. Among planktonic foraminifera, *N. pachyderma sin.* decrease, while boreal *G. bulloides* increase to 15–25%; the appearance of *N. pachyderma dex* indicates relatively warm waters. The interval apparently was deposited during the mid-Holocene climate optimum (Atlantic phase).

Interval 135–0 cm. The PF and BF compositions are similar to those in the 300–135 cm interval though differ in a lower number of dominant species. The assemblage includes 23 benthic species, with a foraminifera number of 28. The PF number is from 15 to 48, with quite a large percentage of boreal *G. bulloides* and with the presence of *N. pachyderma dex* that lives in warm waters. The BF composition is comparable with the modern fauna of the study area (Saidova, 1997; Pletnev et al., 2014), which indicates a late Holocene (Subboreal–Subatlantic) age of the interval.

The distribution of *U. parvocostata* and *G. bulloides* is distinctly symbatic (Fig. 7), while the variations of *N. labra-*

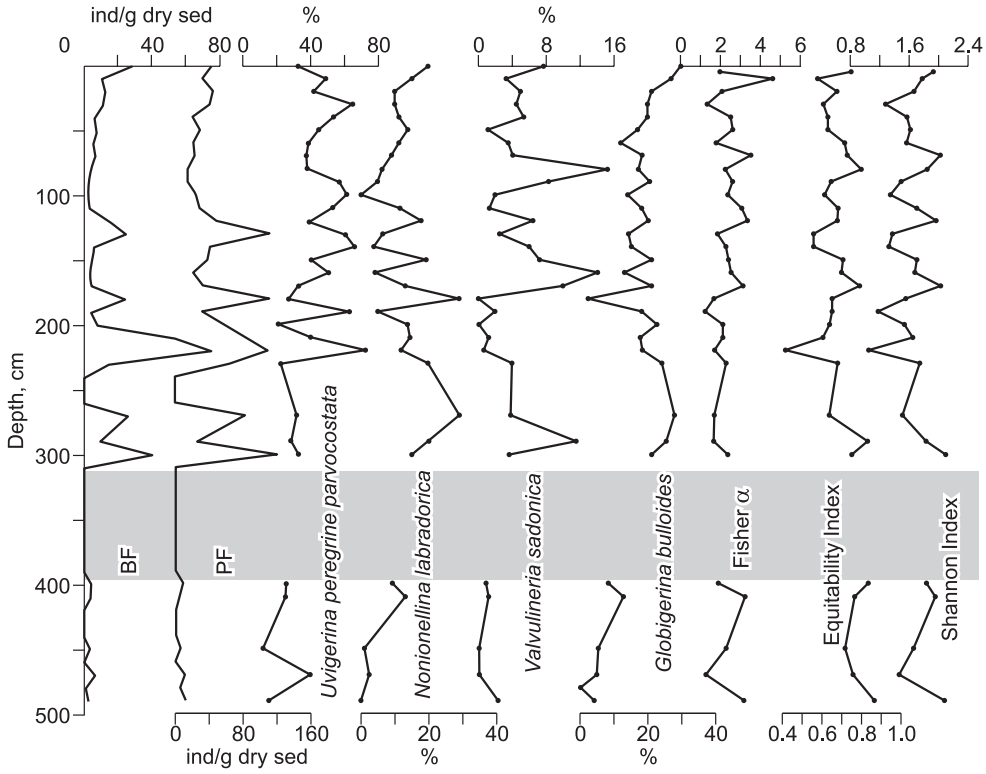

Fig. 7. Foraminifera patterns in core samples: number of individuals per g of dry sediment and percentages of main planktonic and benthic foraminifera species. Diversity indices and equitability are calculated for fossil BF assemblages. Gray color shows intervals of few or absent foraminifera.

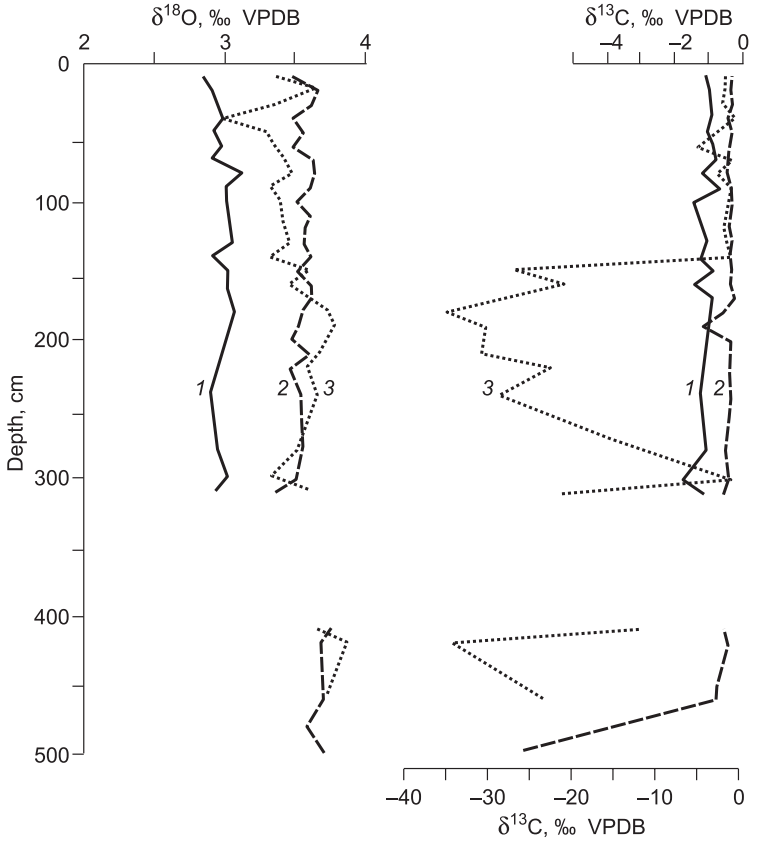

Fig. 8. Oxygen and carbon isotope compositions in different species of benthic foraminifera. *1, V. sadonica; 2*, *U. parvocostata; 3*, *N. labradorica.*

dorica have an opposite pattern. The planktonic species *G. bulloides* is an indicator of high productivity of surface waters (Zaric et al., 2005), while a large flux of organic detritus from the photosynthetic zone maintains high abundance of extant *U. parvocostata* on the bottom (Husid et al., 2013). The endobiont *N. labradorica* lives in deeper waters than *U. parvocostata* and consumes organic matter mainly from pore water (Leiter and Altenbach, 2010).

The diversity and equitability indices that record taxonomic changes in BF assemblages show high diversity during the deposition of two upper units (Fig. 7). The patterns reveal alternating oxic-suboxic conditions in bottom water, most likely controlled by the variations of monsoon-type climate and the Amur discharge.

Stable isotope compositions of foraminifera. The carbon isotope composition of *N. labradorica* and *V. sadonica* endobionts and epibenthic *U. parvocostata* varies from –0.79 to –34.75‰ $\delta^{13}C$ (Fig. 8; Table 2). Some $\delta^{13}C$ values are much lower than the background for the same species (Ishimura et al., 2012; Pletnev et al., 2014). The range of $\delta^{13}C$ lows for *U. parvocostata* and *V. sadonica* is much smaller than $\delta^{13}C$ for *N. labradorica*, except for anomalously low values in *U. parvocostata* between 470 and 475 cm.

The best representative $\delta^{13}C$ curve for *N. labradorica* comprises three intervals at 0–135, 135–300 and 300–495 cm of core depth which differ in $\delta^{13}C$ ranges and in colors and preservation of foraminifera and are consistent with lithological and biostratigraphic units.

The upper interval (0–135 cm) includes three negative $\delta^{13}C$ excursions in *N. labradorica* at 40–45, 50–55 and 70–75 cm: –2.52‰, –5.10‰ and –2.82‰, respectively. The tests are white and transparent, without signatures of secondary calcification detectable in SEM images (Plate 1). The $\delta^{13}C$ values are 0.3–0.5 ‰ lower at 30–35 and 60–75 cm in *U. parvocostata* and slightly lower also at 90–95 cm in *V. sadonica*.

The interval 140–270 cm for *N. labradorica* is marked by a single negative $\delta^{13}C$ excursion to –34.75‰. The –1 to –1.7‰ values at 170, 210, 240, and 290 cm for *U. parvocostata* and at 150 and 290 cm for *V. sadonica* indicate periodic methane emissions during the deposition. The –3.82‰ $\delta^{13}C$ excursion for *Uvigerina parvocostata* coincides with the main peak in *N. labradorica*. The minimum values for both species evidence of a strong MDAC impact. Some tests from 140–150 and 170–230 cm have secondary calcic overgrowths.

In the lower interval (300–495 cm), *N. labradorica* shows a prominent negative $\delta^{13}C$ excursion to –34.97‰ at 410 cm. The medium and lower intervals are divided by a layer at 290–300 cm where the values for *N. labradorica* (–1.7‰) correspond to normal marine conditions. *U. parvocostata* shows depleted $\delta^{13}C$ of <–2‰ over the whole interval, espe-

Table 2. $\delta^{18}O$ and $\delta^{13}C$ patterns in three types of benthic foraminifera in core LV50-05

Depth, cm	Species	Size of tests, mm	$\delta^{13}C$, ‰ VPDB	$\delta^{18}O$, ‰ VPDB
10—15	*U. parvocostata*	1.0	–1.08	3.65
10—15	*N. labradorica*	0.5—0.6	–1.92	3.40
20—25	*U. parvocostata*	1.0	–0.93	3.61
20—25	*V. sadonica*	0 .6—0.8	–1.00	2.91
20—25	*N. labradorica*	0.35—0.6	–2.13	3.36
30—35	*U. parvocostata*	1.0	–1.42	3.48
30—35	*V. sadonica*	0.6—0.7	–0.92	2.99
30—35	*N. labradorica*	0.4—0.7	–0.86	3.02
40—45	*U. parvocostata*	1.0	–0.99	3.55
40—45	*V. sadonica*	0.45—0.7	–0.94	2.93
40—45	*N. labradorica*	0.4—0.55	–2.52	3.30
50—55	*U. parvocostata*	1.0	–1.18	3.48
50—55	*V. sadonica*	0.6—0.7	–0.85	2.98
50—55	*N. labradorica*	0.5—0.6	–5.11	3.36
60—65	*U. parvocostata*	1.0	–1.44	3.61
60—65	*V. sadonica*	0.5—0.6	–0.79	2.91
60—65	*N. labradorica*	0.5—0.6	–1.27	3.43
70—75	*U. parvocostata*	1.0	–1.48	3.63
70—75	*V. sadonica*	0.6—0.7	–1.18	3.11
70—75	*N. labradorica*	0.4—0.6	–2.82	3.48
80—85	*U. parvocostata*	1.0	–0.95	3.60
80—85	*V. sadonica*	0.4—0.75	–0.68	3.01
80—85	*N. labradorica*	0.4—0.5	–1.36	3.34
90—95	*U. parvocostata*	1.0	–1.02	3.51
90—95	*V. sadonica*	0.4—0.7	–1.40	3.01
90—95	*N. labradorica*	0.4—0.6	–1.60	3.39
100—105	*U. parvocostata*	1.0	–1.20	3.60
110—115	»	1.0	–1.33	3.56
110—115	*N. labradorica*	0.3—0.5	–2.18	3.44
120—125	*U. parvocostata*	1.0	–1.03	3.56
120—125	*V. sadonica*	0.6—0.7	–1.00	3.05
120—125	*N. labradorica*	0.5—0.6	–1.68	3.47
130—135	*U. parvocostata*	1.0	–1.04	3.60
130—135	*V. sadonica*	0.5—0.7	–1.15	2.92
130—135	*N. labradorica*	0.4—0.6	–1.40	3.34
140—145	*U. parvocostata*	1.0	–0.98	3.51
140—145	*V. sadonica*	0.5—0.8	–0.84	3.02
140—145	*N. labradorica*	0.5	–26.56	3.60
150—155	*U. parvocostata*	1.0	–1.07	3.60
150—155	*V. sadonica*	0.6—0.8	–1.42	3.02
150—155	*N. labradorica*	0.5	–21.52	3.48
160—165	*U. parvocostata*	1.0	–0.79	3.61
160—165	*V. sadonica*	0.3—0.7	–0.89	3.04
170—175	*U. parvocostata*	1.0	–1.83	3.54
170—175	*V. sadonica*	0.6—0.7	–0.93	3.07
170—175	*N. labradorica*	0.5—0.6	–34.75	3.74
180—185	*U. parvocostata*	1.0	–3.82	3.51
180—185	*N. labradorica*	0.6	–30.55	3.78
190—195	*U. parvocostata*	1.0	–1.08	3.47
200—205	»	1.0	–1.19	3.58
200—205	*N. labradorica*	0.5—0.7	–30.83	3.67
210—215	*U. parvocostata*	1.0	–1.34	3.47
210—215	*N. labradorica*	0.5—0.6	–22.93	3.59
230—235	*U. parvocostata*	1.0	–1.17	3.53

(*continued on next page*)

Table 2 (*continued*)

Depth, cm	Species	Size of tests, mm	$\delta^{13}C$, ‰ VPDB	$\delta^{18}O$, ‰ VPDB
230—235	*V. sadonica*	0.6–0.8	–1.22	2.90
230—235	*N. labradorica*	0.5	–28.89	3.66
270—275	*U. parvocostata*	1.0	–1.68	3.55
270—275	*V. sadonica*	0.6–0.8	–1.08	2.95
270—275	*N. labradorica*	0.6	–11.88	3.54
290—295	*U. parvocostata*	1.0	–1.49	3.50
290—295	*V. sadonica*	0.5–0.6	–1.71	3.02
290—295	*N. labradorica*	0.5	–1.70	3.35
300—305	*U. parvocostata*	1.0	–1.97	3.35
300—305	*V. sadonica*	0.6–0.7	–1.10	2.94
300—305	*N. labradorica*	0.5–0.6	–21.20	3.61
400—405	*U. parvocostata*	1.0	–2.10	3.75
400—405	*N. labradorica*	0.6–0.7	–11.91	3.66
410—420	*U. parvocostata*	1.0	–1.75	3.68
410—420	*N. labradorica*	0.6–0.7	–34.97	3.86
450—455	*U. parvocostata*	1.0	–3.23	3.70
470—475	»	1.0	–3.47	3.59
470—475	*N. labradorica*	0.5	–23.70	3.72
490—495	*U. parvocostata*	1.0	–25.97	3.71

cially in the lower part (450–495 cm). The low of –25.97‰ $\delta^{13}C$ for *U. parvocostata* is recorded within 470–495 cm where foraminifera are corroded and brown stained (Plate 1).

The $\delta^{18}O$ values in benthic foraminifera vary insignificantly (Fig. 8; Table 2) which is evidence of stable bottom water temperatures in the past. As it was shown earlier (Torres et al., 2003; Uchida et al., 2008; Pearson, 2012), $\delta^{18}O$ is sometimes 0.3–0.5‰ heavier in the tests with depleted $\delta^{13}C$. In the core LV50-05, the effect was observed at 170, 270 and 410 cm core depths in *U. parvocostata.*

DISCUSSION

The $\delta^{13}C$ excursions from –1.5 to –34‰ in *N. labradorica* and *U. parvocostata, V sadonica* in the LV50-05 core are markedly more negative than the background values of the same foraminifera species that live outside the zones of methane seeps in the Sea of Okhotsk. These lows are explicitly or implicitly related to increasing methane concentrations in bottom sediments during the lifetime of the foraminifera, and we call them *methane events* (ME). The foraminiferal $^{13}C/^{12}C$ ratios in tests, along with lithostratigraphic and biostratigraphic data and AMS ^{14}C ages, reveal several methane events in the core separated by spells of normal marine $\delta^{13}C$: ME-1 (700 to 900 years BP); ME-2 (1200 to 1400 years BP); ME-3 (2500 to 5400 years BP), and ME-4 (7400 to 10000 years BP) (Fig. 9).

Picking the main (live) and postdepositional $\delta^{13}C$ signals in the foraminifera records is the key deciphering issue. The methane response in the record of alive foraminifera is slightly lower than the respective values outside the methane seeps (Sen Gupta et al., 1997; Torres et al., 2003; Bernard et al., 2010). Our analysis of isotopes in live benthic foraminifera of three species from the LV50 site in the Sea of Okhotsk showed variations from –0.3 to –1‰ (Pletnev et al., 2014). The live $\delta^{13}C$ methane response of the Sea of Okhotsk species is from –1.4 to –1.6‰ for *U. parvocostata* and *V. sadonica* and from –2.0 to –3.0‰ for *N. labradorica* (Pletnev et al., 2017). The range for *N. Labradorica* may be larger because it can tolerate the conditions of methane seeps at the LV-50 site. The same $\delta^{13}C$ difference between and within foraminifera species likely persisted in the Holocene. The main rsponse may be often masked by a stronger MDAC signal (Aharon et al., 1997; Torres et al., 2003; Uchida et al., 2008): the most prominent $\delta^{13}C$ excursions correspond to MDAC effects in our data. There is evidence that the $\delta^{13}C$ values below –1.6‰ bear MDAC signatures (Ambrose et al., 2015).

The $\delta^{13}C$ variations for *N. labradorica* (Figs. 8, 9; Table 2) are especially interesting. The negative $\delta^{13}C$ excursions at 40–45 cm (–2.5‰) and 70–75 cm (–2.8‰) mark two brief events ME-1 and ME-2 which record the live signal during methane emission. The $\delta^{13}C$ values of *N. labradorica* during the ME-3 and ME-4 events were 4–6 times as low as during ME-1 and ME-2. The main and secondary signals of early emissions are hard to discriminate. Low $\delta^{13}C$ unambiguously indicate a greater role of MDAC during ME-3 and ME-4 than during ME-1 and ME-2. Traces of secondary calcification are well evident both under the binocular and in SEM images. MDAC effects also show up in a negative $\delta^{13}C$ excursion of –5.1‰ for *N. labradorica* at 50–55 cm.

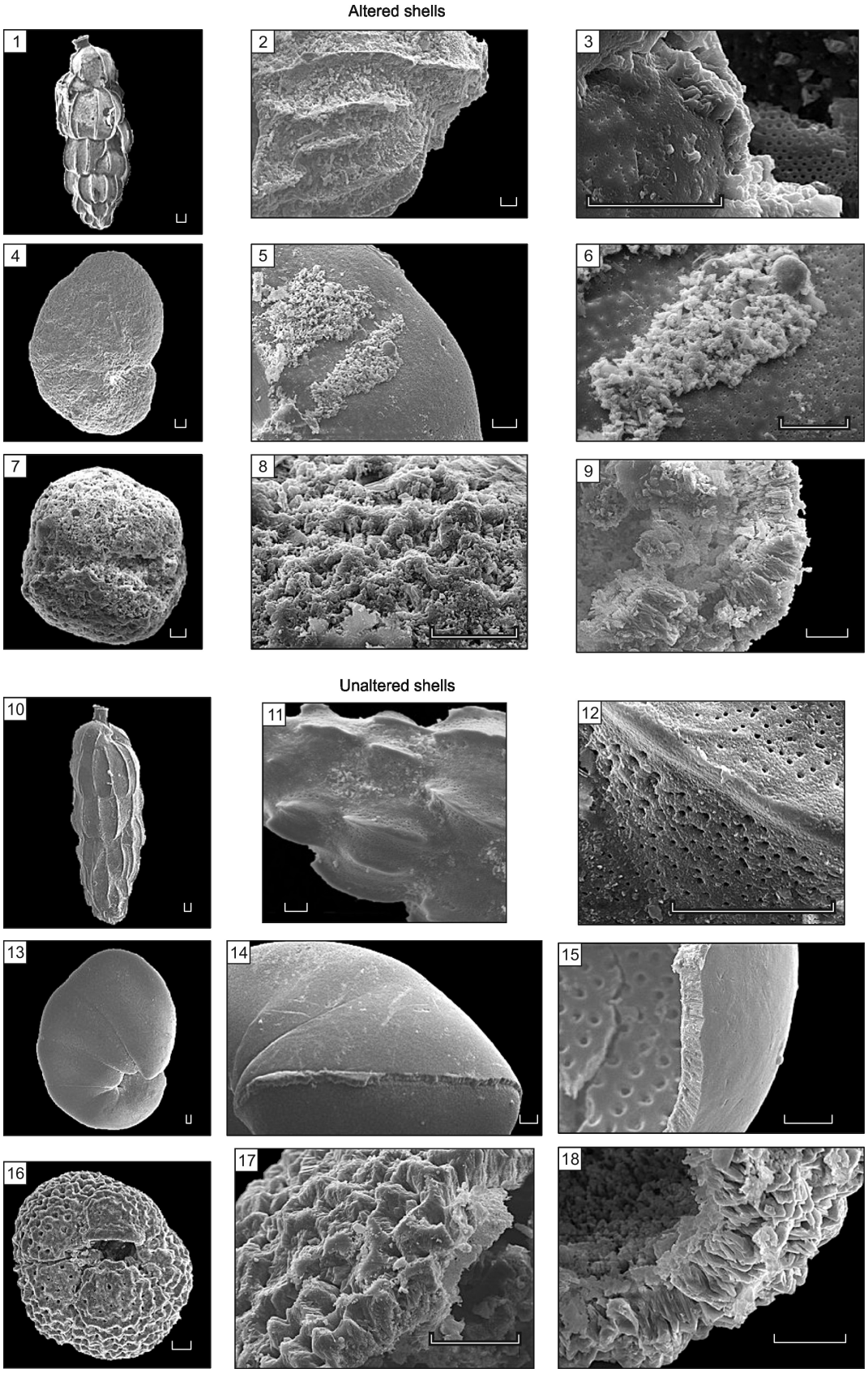

Plate 1. SEM images of benthic species: *U. peregrina parvocostata* (1–3; 10–12), *N. labradorica* (4–6; 13–15) and planktonic *N. pachyderma sin* (7–9; 16–18). Upper images (1–9): foraminifera affected by MDAC from intervals 450–455 and 490–495 cm. Lower images (10–18): unaltered foraminifera from intervals 50–55 cm in core LV 50-05. Scale bar is 10 μm.

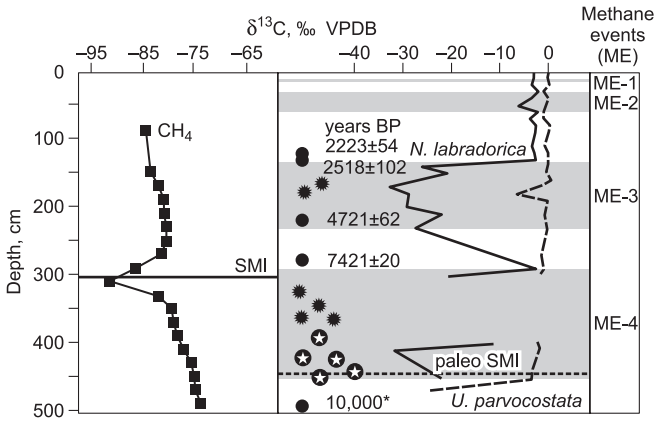

Fig. 9. Position of present SMI (left) and $\delta^{13}C$ in pore water methane (Hachikubo, Kitami Institute of Technology, Japan, pers. commun.); AMS C^{14} ages and depth-dependent $\delta^{13}C$ variations in *N. labradorica* and *U. parvocostata* (right). Gray color shows intervals of methane events.

Previously negative $\delta^{13}C$ excursions were reported for *N. labradorica* dated at 3500 and 7000 years BP from two cores from the Sea of Okhotsk (Lembke-Jene et al., 2007) and were attributed mainly to MDAC. These ages fall within the ME-3 and ME-4 spans, i.e., the two events were of regional scale.

$\delta^{13}C$ variations in *U. parvocostata* are well complementary to the $\delta^{13}C$ results for *N. labradorica*: its minimums coincide with or are next to ME-1, MC-2, and MC-3. Importantly, the negative $\delta^{13}C$ excursions for *U. parvocostata* represent the methane record in foraminifera while they were alive, as most $\delta^{13}C$ values are in a threshold range of –1.4 to –1.6‰ (Figs. 8, 9; Table 2), except for the 180–185 cm interval (ME-3), where they reach –3.8‰ as evidence of MDAC. Enhanced activity of currents during ME-3 is indicated by $\delta^{13}C$ signals of *U. parvocostata*, which are times the background value for that period. The MDAC signal increases in ME-4 and overwhelms the main signal in the primary calcite record of this species. The process culminated at –26.0‰ $\delta^{13}C$ in *U. parvocostata* at the depths 470–475 cm, possibly, because authigenic calcite was growing.

The $\delta^{13}C$ values for *V. sadonica* are close to the normal marine level almost throughout the core, and only few minimums confirm emissions during ME-3. This species commonly lives in the Sea of Okhotsk deeper than the sampling depth of the core (Saidova, 1997), and it is less informative and less abundant than *U. parvocostata* and *N. labradorica*.

Foraminiferal $\delta^{13}C$ may also vary under the effect of changing carbon flux from the zone of photosynthesis and carbon transport to the study area by the Amur River and Sea of Okhotsk intermediate waters from northwest. Variations in the counts of *G. bulloides*, a productivity proxy for the photosynthetic zone (Zaric et al., 2005), do not show any notable correlation between the number of species and $\delta^{13}C$ lows (Fig. 7). The Fischer α and Shannon diversity indices, which record fast changes in foraminifera taxonomy caused by oxic to suboxic transitions in the ocean, are high in ME-3–ME-1 but low in ME-4 (Fig. 7). They show that the negative $\delta^{13}C$ excursions do not correlate with oxygen contents in the bottom water. The present $\delta^{13}C_{DIC}$ values at the sea depths from 600 to 1000 m in the area increase with depth only slightly: from –0.3 to –0.5‰ (Itoh et al., 2013), and the variations in the late and middle Holocene were likewise minor in the central Sea of Okhotsk (Lembke-Jene et al, 2017).

Thus, the external natural factors were of secondary importance and could not change markedly the $\delta^{13}C$ of *N. labradorica* and *U. parvocostata* during ME-1–ME-3. Their influence on foraminiferal $\delta^{13}C$ was significant in the Pleistocene, when the climate changed between glacial and interglacial conditions (Wu et al., 2014; Lembke-Jene et al., 2017).

The two species *U. parvocostata* and *N. labradorica* differ in $\delta^{13}C$ because they live in different environments, though both belong to suboxic infauna (Kaiho, 1994). The species of the *Nonionella* genus, close to the Nonionellina suborder, can live within 19 cm depths in bottom sediments (Leiter and Altenbach, 2010); they are better adapted to sulfide environments and feed on organic matter from pore water. Unlike these, *U. parvocostata* live in the top 1–2 cm of sediments and consume primary C_{org}. The diet difference is evident in mirror-like patterns of depth-dependent foraminifera percentages (Fig. 10). The increase in methane flux and the proximity of SMI to the bottom surface could affect the *N. labradorica* endobiont species via pore water.

The isotope signal also depends on the surface of foraminifera tests (whether it is smooth or spinous) and on the volume of the terminal chamber (Pearson, 2012), which has bearing on MDAC formation. The tests of planktonic foraminifera are much more porous than in benthic species (Uchida et al., 2008; Pearson, 2012). The large volume of the terminal chamber in *N. labradorica* may be responsible for a stronger $\delta^{13}C$ signal as MDAC can reside also inside hollow tests.

Microbial methane is an essential agent in the formation and dissociation of gas hydrates in shallow bottom sediments in the area (Hachikubo et al., 2011; Yang et al., 2011). The past and present processes of this kind are traceable according to SMI, which is at the 300 cm level in the core we analyzed. At SMI, pore waters show a –10‰ $\delta^{13}C$ shift (Hachikubo, pers. commun.) and the sediments contain soft carbonate concretions. The interval 430–450 cm (Figs. 3, 10) is rich in hard carbonate concretions and shell fragments of *Calyptogena*, an indicator of chemosynthesis at methane seeps (Levin, 2005). In the Sea of Okhotsk, such concretions have $\delta^{13}C$ from –37 to –46‰, which proves their methane-derived origin (Greinhert and Derkachev, 2004). These findings in the 430–450 cm interval reveal the past SMI position and, on the other hand, prove the existence of methane emissions in ME-4. Possibly, the findings of soft concretions

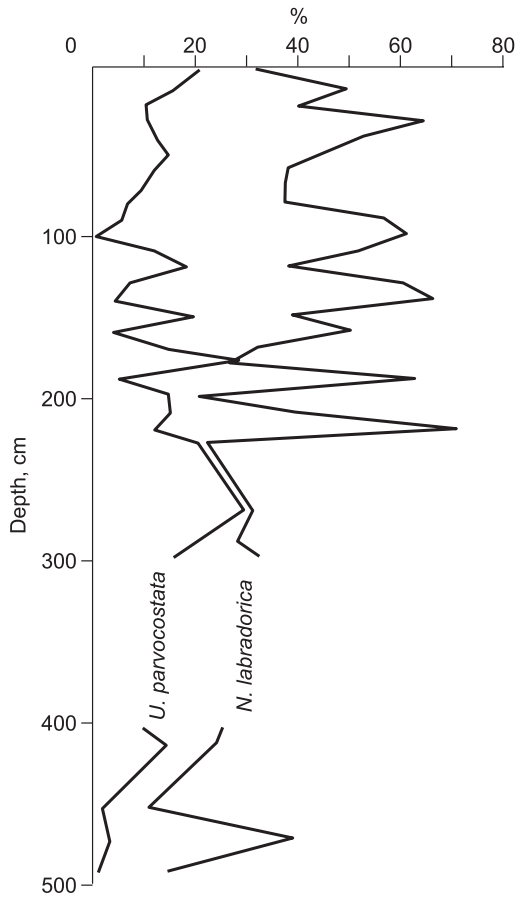

Fig. 10. Distribution of *N. labradorica* and *U. parvocostata* in core LV50.

within 153–154 and 353–356 cm are also markers of SMI. Lithification of soft concretions may be a very long process which could span several successive methane events.

The precipitation of carbonates was accompanied by increase in alkali contents, accelerated formation of CO_3^{2-} (Tishchenko et al., 2005; Ussler and Paull, 2008), and pH changes in pore water (Treude et al., 2005). The pH variations could lead to dissolution of carbonate foraminifera tests and produce mute intervals, as it happened in the LV50-05 core. Previously, such gaps of uncertain origin were reported for foraminiferal records from the Sea of Japan and the Sea of Okhotsk (Pletnev, 2009).

The methane events distinguished in the Sea of Okhotsk may be a response to geological processes of different ages. ME-4 was associated with a dramatic change from the Last Glacial to the Holocene optimum. At 18–15 kyr BP, the sea level may have been 130 m lower than now (Miller et al., 2005), the bottom of shallow straits emerged, and the islands of Sakhalin, Hokkaido, Lesser Kuriles, and Kunashir made up a single continental landmass with the Primorye territory in easternmost Eurasia (Pletnev, 2004). Thus the southwestern Okhotsk Sea became fully isolated from the warm Japan Sea and partly from the Pacific which led to its cooling and formation of gas hydrates (Wong et al., 2003). The *PT* conditions for the gas hydrate formation changed at the onset of global warming and rapid sealevel rise at 15 to 8 kyr BP. Increase in hydrostatic pressure during the Preboreal phase of the Holocene induced dissociation of methane hydrates with release of methane in the Sea of Okhotsk (ME-4), as well as over the Northern Hemisphere as a whole (Maslin et al., 2004; Uchida et al., 2008).

ME-3, in our view, was triggered by a deposition change: biogenic (diatom) sedimentation increased in the middle Holocene (about 7 kyr BP) and reached its maximum during the Atlantic optimum (Seki et al., 2004). The primary productivity and C_{org} flux to the bottom (Seki et al., 2004) increased due to retreat of sea ice, warming of surface water temperatures (Sakamoto et al., 2006), and resumed supply of fresh waters from the Amur River. Furthermore, the flux of carbon increased with permafrost degradation and additional transport by the Amur and intermediate waters. The C_{org} increase and high deposition rates maintained active biogeochemical processes in anaerobic surface sediments and the ensuing microbial methane production. Gas hydrates recovered by gravity coring at the LV50 site consist of biogenic methane (Hachikubo et al., 2011), which might partly be a product of bacterial rework of deep methane, though the latter hardly can have increased much as a result of a 3–5 m sealevel rise in the middle Holocene.

By analogy with the present setting, the carbon isotope composition of foraminifera indicates that normal marine conditions at the coring site have existed for the past 2300 years and were punctuated by brief methane events 2 and 1 in response to natural catastrophes. Methane seepage became times greater after earthquakes (Field and Jennings, 1987) and the large eruption of Paeuktu (Chángbáishān) volcano 938 years ago at the China/Korea boundary fell within ME-1 (Utkin, 2014). The causes of ME-2 remain under study.

We hope that our data on foraminifera as a record of methane emission history will be useful for further studies of gas emissions and paleogeography of the Sea of Okhotsk.

CONCLUSIONS

The CH_4 and SO_4^{2-} profiles in the LV50 core of bottom sediments show that methane venting at the site was of local occurrence. The core intervals deposited in the time when methane emission exceeded the present-day background are recorded in foraminiferal $\delta^{13}C$, AMS ^{14}C, and biostratigraphic data. They are the methane events ME-1 at 700–900 years BP, ME-2 at 1200–1400 years BP, ME-3 at 2500–5400 years BP, and ME-4 at 7400–10000 years BP.

The presence of methane-derived carbonate precipitates and shells of chemosynthetic mollusks in the 430–450 cm interval of the LV50 core marks the past position of SMI and provides evidence for episodic methane seepage in the early Holocene (ME-4).

The methane responses of extant *N. labradorica, U. parvocostata*, and *V. sadonica* make reference for discrimination between the live and postdeposition ME signals in the $\delta^{13}C$ records of fossil foraminifera. The *U. parvocostata* responses mark especially the chronology of methane emissions while *N. labradorica* is more sensitive to the formation of methane-derived carbonate.

In the Sea of Okhotsk, ME-1 and ME-2 were brief episodes that were possibly triggered by active volcanism and earthquakes. The longer event 3 was associated with marked increase in diatom deposition during the Atlantic phase. Enhanced C_{org} in shallow sediments maintained biogeochemical processes and production of biogenic methane. ME-4 occurred in a setting of global sealevel rise in the latest Pleistocene and early Holocene. Increase in the hydrostatic pressure in Preboreal time induced gas hydrate dissociation in the Sea of Okhotsk, as well as globally in the Northern Hemisphere.

We greatly appreciate the opportunity to participate in the cruise LV50 offered by Professor A.I. Obzhirov. We wish to thank A.N. Derkachev and N.A. Nikolaeva (V.I. Ilyichev Pacific Oceanological Institute, Vladivostok) for lithological description of core LV50, A. Hachikubo (Technological Institute, Kitami) for sharing access to chemical analytical database, and Professors Jian Zhimin and Cheng Xinrong for collaboration in isotope analytical work.

The study was supported by grants from the Basic Science Foundation for National Social Research Institutions of China (2012G07, 2013G38), the National Natural Science Foundation of China (40710069004), and the Far East Branch of the Russian Academy of Sciences (15-I-2-063).

The study was carried out as part of government assignment AAAA-A17-117030110035-4.

REFERENCES

Aharon, S.P., Schwarcz, H.P., Roberts, H.H., 1997. Radiometric dating of submarine hydrocarbon seeps in the Gulf of Mexico. Geol. Soc. Amer. Bull. 109 (5), 568–579.

Akulichev, V.A., Obzhirov, A.I., Shakirov, R.B., Maltseva, E.V., Gresov, A.I., Telegin, Yu.A., 2014. Conditions of gas hydrate formation in the Sea of Okhotsk. Dokl. Earth Sci. 454 (1), 94–96.

Ambrose, W.G.Jr., Panieri, G., Schneider, A., Plaza-Faverola, A., Carroll, M.L., Astrom, E.K.L., Locke, W.L., Carroll, J., 2015. Bivalve shell horizons in seafloor pockmarks of the last glacial-interglacial transition: a thousand years of methane emissions in the Arctic Ocean. Geochem. Geophys. Geosyst. 16 (12), 4108–4129.

Anikiev, V.V., Dudarev, O.V., Botsul, A.I., Utkin, I.V., Kolesov, G.M., 2001. Factors of mesoscale variability in the distribution of the particulate matter and chemical elements in the Amur River estuary—Sea of Okhotsk waters. Geochem. Int. 39 (1), 64–87.

Arslanov, Kh.A., 1987. Radiocarbon: Geochemistry and Geochronology [in Russian]. LGU, Leningrad.

Bernhard, J.M., Martin, J.B., Rathburn, A.E., 2010. Combined carbonate carbon isotopic and cellular ultrastructural studies of individual benthic foraminifera. 2: Toward an understanding of apparent disequilibrium in hydrocarbon seeps. Paleoceanogr. Paleoclimatol. 25 (4), PA4206. doi:10.1029/2010PA001930.

Biebow, N., Kulinich, R., Baranov, B., 2003. Cruise Report: KOMEX (Kurile Okhotsk Sea Marine Experiment), RV Akademik M.A. Lavrentyev Cruise 29, Leg 1 and Leg 2. GEOMAR Report. Research Center for Marine Geosciences, Kiel.

Borowski, W.S., Paull, C.K., Ussler III, W., 1999. Global and local variations of interstitial sulfate gradients in deep-water, continental margin sediments: Sensitivity to underlying methane and gas hydrates. Mar. Geol. 159, 131–154.

Cheng, X., Huang, B., Jian, Z., Zhao, Q., Tian, J., Li, J., 2005. Foraminiferal isotopic evidence for monsoonal activity in the South China Sea: a present-LGM comparison. Mar. Micropaleontol. 54 (1–2), 125–139.

Cook, M.S., Keigwin, L.D., Birgel, D., Hinrich, K.U., 2011. Repeated pulses of vertical methane flux recorded in glacial sediments from the southeast Bering Sea. Paleoceanogr. Paleoclimatol. 26 (2), PA2210. doi:10.1029/2010PA001993.

Dickens, G., O'Neil, O., Rea, D., Owen, R., 1995. Dissociation of oceanic methane hydrate as a cause of the carbon isotope excursion at the end of the Paleocene. Paleoceanogr. Paleoclimatol. 10 (6), 965–971. doi:10.1029/95PA02087.

Fairbanks, R.G., Mortlock, R.A., Chiu, T.C., Cao, L., Kaplan, A., Guilderson, T.P., Fairbanks, T.W., Bloom, A.L., 2005. Marine radiocarbon calibration curve spanning 10,000 to 50,000 years BP based on paired $^{230}Th/^{234}U/^{238}U$ and ^{14}C dates on pristine corals. Quat. Sci. Rev. 24, 1781–1796.

Field, M.E., Jennings, A.E., 1987. Seafloor gas seeps triggered by a northern California earthquake. Mar. Geol. 77 (1–2), 39–51.

Freeland, H.J., Bychkov, A.S., Whitney, F., Taylor, C., Wong, C.S., Yurasov, G.I., 1998. WOCE section P1W in the Sea of Okhotsk: 1. Oceanographic data description. J. Geophys. Res. 103 (C8), 15,613–15,623.

Greinert, J., Derkachev, A., 2004. Glendonites and methane-derived Mg-calcites in the Sea of Okhotsk, Eastern Siberia: implications of a venting-related ikaite/glendonite formation. Mar. Ecol. 204 (1–2), 129–144.

Hachikubo, A, Tatsumi, K., Sakagami, H., Minami, H., Yamashita, S., Takahashi, N., Shoji, H., Young, K.J., Vereshchagina, O., Obzhirov, A., 2011. Molecular and isotopic compositions of hydrate-bound hydrocarbons in subsurface sediments from offshore Sakhalin Island, Sea of Okhotsk, in: Proc. 7th Int. Conf. Gas Hydrates (ICGH 2011). Edinburgh, pp. 17–21.

Harper, D.A.T., 1999. Numerical Palaeobiology: Computer-Based Modelling and Analysis of Fossils and Their Distributions. John Wiley&Sons, New York.

Heier-Nielsen, S., Conradsen, K., Heinemeier, J., Knudsen, K.L., Nielsen, H.L., Rud, N., Sveinbjörnsdóttir, A.E., 1995. Radiocarbon dating of shells and foraminifera from the Skagen Core, Denmark: Evidence of reworking. Radiocarbon 37 (2), 119–130.

Hill, T.M., Stott, L., Valentine, D.L., 2004. Isotopic evidence for the incorporation of methane-derived carbon into foraminifera from modern methane seeps, Hydrate Ridge, Northeast Pacific. Geochim. Cosmochim. Acta 68 (22), 4619–4627.

Hoefs, J., 1980. Stable Isotope Geochemistry. Springer Verlag, Berlin-Heidelberg.

Husid, T.A., Belaeva, N.V., Demina, L.L., Domanov, M.M., Chekhovskaya, M.P., 2013. Changes in assemblages of planktonic and benthic foraminifera in the Upper Quaternary deposits of the Deryugin Basin, Sea of Okhotsk. Stratigrafiya, Geologicheskaya Korrelatsiya 21 (2), 110–121.

Ishimura, T., Tsunogai, U., Hasegawa, S., Nakagawa, F., Oi, T., Kitazato, H., 2012. Variation in stable carbon and oxygen isotopes of individual benthic foraminifera: tracers for quantifying the vital effect. Biogeosci. Discuss 9, 6191–6218.

Itoh, M., Ohshima, K.I., Wakatsuchi, M., 2003. Distribution and formation of Okhotsk Sea Intermediate Water: An analysis of isopycnal climatological data. J. Geophys. Res. 108 (C8), 3258. doi:10.1029/2002JC001590.

Kaiho, K., 1994. Benthic foraminiferal dissolved-oxygen index and dissolved-oxygen levels in the modern ocean. Geology 22 (8), 719–722.

Keigwin, L.D., 1998. Glacial-age hydrography of the far northwest Pacific Ocean. Paleoceanogr. Paleoclimatol. 13 (4), 323–339.

Kennett, J., Cannariato, K., Hendy, I., Behl, R., 2000. Carbon isotopic evidence for methane hydrate instability during Quaternary interstadials. Science 288, 128–133.

Kharakhinov, V.V., 2010. Petroleum Geology of the Sakhalin Region [in Russian]. Nauchnyi Mir, Moscow.

Kim, Y.-G., Lee, S.-M., Jin, Y.K., Baranov, B., Obzhirov, A., Salomatin, A., Shoji, H., 2013. The stability of gas hydrate field in the northeastern continental slope of Sakhalin Island, Sea of Okhotsk, as inferred from analysis of heat flow data and its implications for slope failures. Mar. Pet. Geol. 45, 198–207.

Kitani, K., 1973. An oceanographic study of the Okhotsk Sea: particularly in regard to cold waters. Bull. Far Seas Fish Res. Lab. 9, 45–77.

Leiter, C., Altenbach, A.V., 2010. Benthic foraminifera from the diatomaceous mud belt off Namibia: Characteristic species for severe anoxia. Palaeontologia Electronica 13 (2), 11A. http://palaeo-electronica.org/2010_2/188/index.html.

Levin, L.A., 2005. Ecology of cold seep sediments: Interactions of fauna with flow, chemistry and microbes. Oceanogr. Mar. Biol. Annu. Rev. 43, 1–46.

Lembke-Jene, L., Tiedemann, R., Nuernberg, D., Obzhirov, A., Dullo, C., 2007. Variable Holocene methane emissions from cold seeps in the Okhotsk Sea–links to seismo-tectonic activity. Geophys. Res. Abstr. 9, 10177.

Lembke-Jene, L, Tiedemann, R., Nürnberg, D., Kokfelt, U., Kozdon, R., Max, L., Röhl, U., Gorbarenko, S.A., 2017. Deglacial variability in Okhotsk Sea Intermediate Water ventilation and biogeochemistry: Implications for North Pacific nutrient supply and productivity. Quat. Sci. Rev. 160, 116–137.

Logvina, E.A., Prasolov, E.M., Arslanov, Kh.A., Matveeva, T.V., Chernov, S.B., Maksimov, F.E., 2012. Correction of radiocarbon ages of carbonates at hydrothermal vents. Geokhimiya, No. 11, 1064–1069.

Maslin, M., Owen, M., Day, S., Long, D., 2004. Linking continental-slope failures and climate change: Testing the clathrate gun hypothesis. Geology 32 (1), 53–56.

Miller, K.G., Kominz, M.A., Browning, J.V., Wright, J.D., Moutain, G.S., Katz, M.E., Sugarman, P.J., Cramer, B.S., Christie-Blick, N., Pekar, S.F., 2005. The Phanerozoic record of global sea-level change. Science 310, 1293–1298.

Minami, H., Tatsumi, K., Hachikubo, A., Yamashita, S., Sakagami, H., Takahashi, N., Shoji, H., Jin, Y.K., Obzhirov, A., Nikolaeva, N., Derkachev, A., 2012. Possible variation in methane flux caused by gas hydrate formation on the northeastern continental slope off Sakhalin Island, Russia. Geo-Mar. Lett. 32 (5–6), 525–534.

Panieri, G., Aharon, P., Sen Gupta, B.K., Camerlenghi, A., Ferrer, F.P., Cacho, I., 2014. Late Holocene foraminifera of Blake Ridge diapir: Assemblage variation and stable-isotope record in gas-hydrate bearing sediments. Mar. Geol. 353, 99–107.

Panieri, G., Graves, C., James, R., 2016. Paleo-methane emissions recorded in foraminifera near the landward limit of the gas hydrate stability zone offshore western Svalbard. Geochem. Geophys. Geosyst. 17 (2), 521–537.

Pearson, P., 2012. Oxygen isotopes in foraminifera: overview and historical review reconstructing Earth's deep-time climate–the state of the art in 2012, in: Ivany, L.C., Huber, B.T. (Eds.). Paleontological Society Short Course (November 3, 2012). The Paleontological Society Papers, Vol. 18. Boulder, pp. 1–38.

Pletnev, S.P., 2004. Last isolation of Kuril Island as a result of postglacial transgression. Pices Sci. Rep. 26, 36–37.

Pletnev, S.P., 2009. Depths of the Sea of Okhotsk sedimentary basin in the Cenozoic. Russ. J. Pacific Geol. 3, 118–127.

Pletnev, S.P., Annin, V.K., Wu, Y., Tarasova, T.S., 2014. Foraminifera associated with cold methane seeps in the eastern slope off Sakhalin (Sea of Okhotsk): oxygen and carbon isotope compositions ($\delta^{18}O$ and $\delta^{13}C$). Izvestiya TINRO 178, 180–190.

Pletnev, S.P., Romanova, A.V., Wu, Y., Annin, V.K., Utkin, I.V., Vereshchagina, O.F., 2017. Negative δ13C excursions and methane emissions in the southwestern Sea of Okhotsk for the past 10 000 years, in: Proc. 22nd Int. Conf. Mar. Geol. (Moscow, 20–24 November 2017) [in Russian]. GEOS, Moscow, Book 1, pp. 216–218.

Rathburn, A.E., Levin, L., Held, Z., Lohmann, K.C., 2000. Benthic foraminifera associated with cold methane seeps on the northern California margin: Ecology and stable isotopic composition. Mar. Micropaleontol. 38 (3–4), 247–266.

Rathburn, A.E., Perez, M.E., Martin, J.B., Day, S.A., Mahn, C., Gieskes, J., Ziebis, W., Williams, D., Bahls, A., 2003. Relationship between the distribution and stable isotopic composition of living benthic foraminifera and cold methane seep biogeochemistry in Monterey Bay, California. Geochem. Geophys. Geosyst. 4 (12), 1106. doi:10.1029/ 2003GC000595.

Saidova, Kh.M., 1997. Pelagic foraminifera communities in the Bering and Okhotsk Seas. Okeanologiya 37 (3), 105–112.

Sakamoto, T., Ikehara, M., Uchida, M., Aoki, K., Shibata, Y., Kanamatsu, T., Harada, N., Iijima, K., Katsuki, K., Asahi, H., Takahashi, K., Sakai, H., Kawahata, H., 2006. Millennial-scale variations of sea-ice expansion in the southwestern part of the Okhotsk Sea during the past 120 kyr: age model and ice-rafted debris in IMAGES Core MD01-2412. Global Planet. Change 53, 58–77.

Sen Gupta, B.K., Platon, E., Bernhard, J.M., Aharon, P., 1997. Foraminiferal colonization of hydrocarbon-seep bacterial mats and underlying sediment, Gulf of Mexico slope. J. Foraminifer. Res. 27 (4), 292–300.

Seki, O., Ikehara, M., Kawamura, K., Nakatsuka, T., Ohnishi, K., Wakatsuchi, M., Narita, H., Sakamoto, T., 2004. Reconstruction of paleoproductivity in the Sea of Okhotsk over the last 30 kyr. Paleoceanogr. Paleoclimatol. 19 (1), PA1016. doi:10.1029/2002PA000808.

Shoji, A., Jin, Y.K., Obzhirov, A., Baranov B., 2011. Operation Report of Sakhalin Slope Gas Hydrate Project 2010, R/V Akademik M.A. Lavrentyev, Cruise 50/2011.

Solov'ev, V.A., Ginzburg, G.D., Obzhirov, A.I., Douglas, V.K., 1994. Gas hydrates of the Sea of Okhotsk. Otechestvennaya Geologiya 2, 190–197.

Sorokin, Y.I., Sorokin, P.Y., 1999. Production in the Sea of Okhotsk. J. Plankton Res. 21 (2), 201–230.

Tishchenko, P., Hensen, C., Wallmann, K., Wong, C.S., 2005. Calculation of the stability and solubility of methane hydrate in seawater. Chem. Geol. 219 (1–4), 37–52.

Torres, M.E., Mix, A.C., Kinports, K., Haley, B., Klinkhammer, G.P., McManus, J., de Angelis, M.A., 2003. Is methane venting at the seafloor recorded by $\delta^{13}C$ of benthic foraminifera shells? Paleoceanogr. Paleoclimatol. 18 (3), 1062–1074.

Tsunogai, S., Watanabe, S., Honda, M., Aramaki, T., 1995. North Pacific Intermediate Water studied chiefly with radiocarbon. J. Oceanogr. 51, 519–536.

Treude, T., Niggemann, J., Kallmeyer, J., Wintersteller, P., Schubert, C.J., Boetius, A., Jorgensen, B.B., 2005. Anaerobic oxidiation of methane in the sulfate-methane transition along the Chilean continental margin. Geochim. Cosmochim. Acta 69 (11), 2767–2779.

Uchida, M., Ohkushi, K., Kimoto, K., Inagaki, F., Ishimura, T., Tsunogai, U., Tuzino, T., Shibata, Y., 2008. Radiocarbon-based carbon source quantification of anomalous isotopic foraminifera in last glacial sediments in the western North Pacific. Geochem. Geophys. Geosyst. 9 (4). doi:10.1029/2006GC001558.

Ussler III, W., Paull, C.K., 2008. Rates of anaerobic oxidation of methane and authigenic carbonate mineralization in methane-rich deep-sea sediments inferred from models and geochemical profiles. Earth Planet. Sci. Let. 266 (3–4), 271–287.

Utkin, I.V., 2014. Reconstructing the setting for deposition of distal tephra in the Sea of Japan Basin: A catastrophic eruption of Baitoushan Volcano. J. Volcanol. Seismol. 8 (4), 228–238.

Wong, H.K., Lüdmann, T., Baranov, B.V., Karp, B.Y., Konerding, P., Ion, G., 2003. Bottom current-controlled sedimentation and mass wasting in the northwestern Sea of Okhotsk. Mar. Geol. 201 (4), 287–305.

Wu, Y., Shi, X., Zou, J., Cheng, Z., Wang, K., Ge, S., Shi, F., 2014. Benthic foraminiferal δ^{13} minimum events in the southeastern Okhotsk Sea over the last 180 ka. Chin. Sci. Bull. 59 (24), 3066–3074.

Yang, J.-Y., Chung, K.H., Jin, Y.-K., Shin, K.-H., 2011. Characterizing lipid biomarkers in methanotrophic communities of gas hydrate-bearing sediments in the Sea of Okhotsk. Mar. Pet. Geol. 28 (10), 1884–1898.

Zaric, S., Donner, B., Fischer, G., Mulitza, S., Wefer, G., 2005. Sensitivity of planktonic foraminifera to sea surface temperature and export production as derived from sediment trap data. Mar. Micropaleontol. 55 (1–2), 75–105.

Zonenshain, L.P., Mooredmaa, I.O., Baranov, B.V., Kuznetsov, A.P., Kuzin, V.S., Kuzmin, M.I., Avdeiko, G.P., Stunzhas, P.A., Lukashin, V.N., Barash, M.S., Valashko, G.M., Demina, L.L., 1987. A submarine gas source in the Sea of Okhotsk west of Paramushir Island. Okeanologiya, No. 5, 795–800.

Editorial responsibility: B.N. Shurygin